

# Number of Solution States of Bradykinin from Ion Mobility and Mass Spectrometry Measurements

Nicholas A. Pierson,<sup>†</sup> Liuxi Chen,<sup>‡</sup> Stephen J. Valentine,<sup>†</sup> David H. Russell,<sup>‡</sup> and David E. Clemmer<sup>\*,†</sup>

<sup>†</sup>Department of Chemistry, Indiana University, 800 East Kirkwood Avenue, Bloomington, Indiana 47405, United States

<sup>‡</sup>Department of Chemistry, Texas A&M University, College Station, Texas 77842-3012, United States

**ABSTRACT:** Ion mobility and mass spectrometry measurements have been used to examine the populations of different solution structures of the nonapeptide bradykinin. Over the range of solution compositions studied, from 0:100 to 100:0 methanol:water and 0:100 to 90:10 dioxane:water, evidence for 10 independent populations of bradykinin structures in solution is found. In some solutions as many as eight structures may coexist. The solution populations are substantially different than the gas-phase equilibrium distribution of ions, which exhibits only three distinct states. Such a large number of coexisting structures explains the inability of traditional methods of characterization such as nuclear magnetic resonance spectroscopy and crystallography to determine detailed structural features for some regions of this peptide.

Ion mobility spectrometry (IMS) measurements of bradykinin (BK) ions show vast changes in the number (and relative abundance) of peaks when the solution composition is changed. By comparing with populations that are known for the gas-phase quasi-equilibrium distribution of states,<sup>1</sup> we find that the changes with solution composition must correspond to different numbers of structures in solution. It appears that during the electrospray ionization (ESI)<sup>2</sup> process, populations of structures that are associated with solution equilibria are stabilized as solvent is removed, and the different species can be delineated on the basis of differences in their gas-phase collision cross sections.<sup>3</sup> The evaporative cooling that occurs during the ESI-drying process leads to a freezing-out of different populations,<sup>4,5</sup> making the gas-phase determination of the number of existing solution states highly complementary to efforts to determine conformations in solution by traditional methods.

The BK nonapeptide (Arg<sup>1</sup>–Pro<sup>2</sup>–Pro<sup>3</sup>–Gly<sup>4</sup>–Phe<sup>5</sup>–Ser<sup>6</sup>–Pro<sup>7</sup>–Phe<sup>8</sup>–Arg<sup>9</sup>) is a member of the kinins, a set of molecules discovered in 1909 that possess hypotensive activity.<sup>6</sup> It was isolated in 1956,<sup>7</sup> synthesized in 1960,<sup>8</sup> and has been studied extensively because of its pain-producing effect, involvement in inflammation, and close association with numerous physiological conditions, including sepsis, asthma, myocardial infarctions, and hyperalgesia.<sup>9–11</sup> Despite the tremendous interest in this molecule, only a fraction of its structure is characterized in detail. Circular dichroism,<sup>12</sup> Raman spectroscopy,<sup>13</sup> nuclear magnetic resonance,<sup>14</sup> and molecular modeling studies reveal that the BK Ser<sup>6</sup>–Pro<sup>7</sup>–Phe<sup>8</sup>–Arg<sup>9</sup> residues favor a  $\beta$ -turn motif,<sup>15</sup> whereas the region Arg<sup>1</sup>–Phe<sup>5</sup> is apparently unstructured. This combination of ordered and disordered regions hinders a complete determination of the BK structure. Here, we

show that at least 10 different conformers exist across the range of solutions that are typically used to investigate BK. This plurality suggests that the uncharacterized Arg<sup>1</sup>–Phe<sup>5</sup> region favors specific structures, but no single state dominates to the point that detailed geometries can be determined.

Figure 1 shows IMS distributions, plotted as collision cross sections ( $\Omega$ ),<sup>16</sup> for [BK+3H]<sup>3+</sup> ions that are typical upon electrospraying  $\sim 10^{-6}$ – $10^{-4}$  M BK from 21 different methanol:water and 37 different dioxane:water solutions. These data were recorded with a home-built  $\sim 2$ -m-long drift tube that was filled with  $3.00 \pm 0.02$  Torr of He (300 K) and utilized a drift field of  $10.0 \text{ V} \cdot \text{cm}^{-1}$ . IMS separations are often sensitive to differences in structures of the gas-phase ions.<sup>3,16–18</sup> It is noteworthy that ESI of these solutions also produces [BK+2H]<sup>2+</sup>. Here, we focus on [BK+3H]<sup>3+</sup> because many different structures are resolved. The IMS distribution for [BK+2H]<sup>2+</sup> is dominated by a single broad peak, although field-asymmetric IMS measurements resolve six structures for this ion.<sup>19</sup> As observed in Figure 1, the IMS distributions for [BK+3H]<sup>3+</sup> contain three sharp peaks (at  $\Omega = 269, 285, \text{ and } 305 \text{ \AA}^2$ ) corresponding to the gas-phase structures A, B, and C, assigned previously.<sup>1</sup> A close examination of these data shows that as the solution is changed, these peaks vary in abundance. For example, in the methanol:water data set peak B is favored from 100% methanol solutions; C is favored in more aqueous solutions.

In addition to these sharp features, some solutions produce ions having larger cross sections, extending to  $\sim 350 \text{ \AA}^2$ . The methanol:water system shows that at least three reproducible features exist as elongated forms as the methanol concentration is increased. Significant populations of ions having larger cross sections are observed in dioxane:water solutions; additionally, the relative abundances of these peaks vary dramatically with solution composition. For example, ions with the largest cross section ( $\Omega = 348 \text{ \AA}^2$ ) exhibit a remarkable dependence on the solution composition; they first appear when as little as 5% dioxane is added, decrease as dioxane is increased to  $\sim 20\%$ , and subsequently increase and decrease again (from  $\sim 30$  to 60% dioxane).

More insight into the origin of these peaks can be obtained by comparing these distributions with those that are known to correspond to structures that are formed in the gas phase.<sup>1</sup> Using IMS–IMS techniques (described in detail elsewhere<sup>20</sup>) it is possible to select and activate any of the peaks shown in Figure 1. The activation energy that is used is above all barriers associated with transitions between states but below the energy required for dissociation. This process results in a heating and cooling

Received: April 27, 2011

Published: August 10, 2011

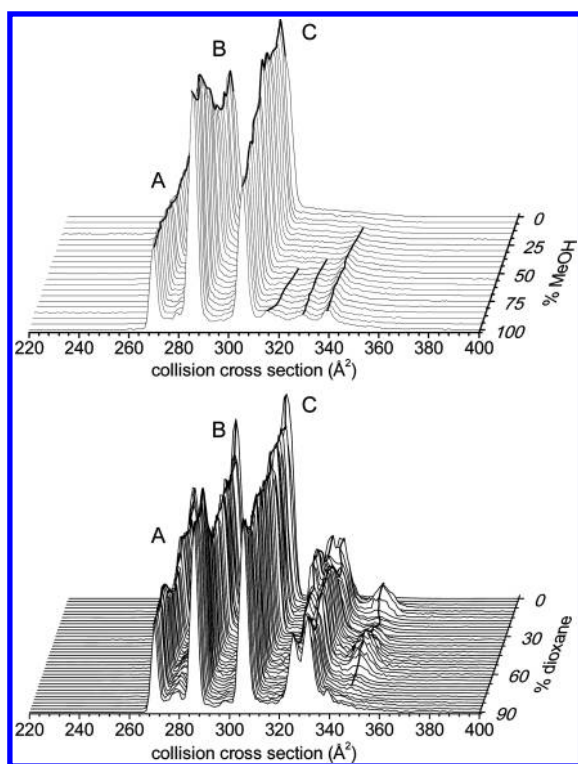


**Figure 1.** IMS distributions of  $[\text{BK}+3\text{H}]^{3+}$  from 21 different methanol:water (top) and 37 different dioxane:water (bottom) solutions, plotted on a collision cross section scale. These data represent the average of three data sets. Abundant conformers A–C are labeled. Peak maxima are connected with solid lines to illustrate changes in conformation abundances.

cycle that effectively anneals selected structures into more stable forms.<sup>18</sup> The uppermost trace in Figure 2 is typical of that obtained upon selection of any of the 10 reproducible peak maxima that are formed under different solution conditions. This is the gas-phase quasi-equilibrium distribution of states.<sup>1</sup> It is dominated by the B ( $\Omega = 285 \text{ \AA}^2$ ) and C ( $\Omega = 305 \text{ \AA}^2$ ) structures, which comprise  $\sim 16 \pm 3$  and  $80 \pm 2\%$  of the gas-phase ion population, respectively; additionally, some more-compact features [including peak A ( $\Omega = 269 \text{ \AA}^2$ )] account for the remaining  $2 \pm 0.3\%$  of the population. That our present data appear so different than the gas-phase quasi-equilibrium distribution requires that there are substantial barriers between the ions that are initially formed from different solutions and those gas-phase structures that are favored upon annealing in the absence of solvent.

As can be observed from Figure 2, BK distributions from several example solution conditions (0:100  $\text{CH}_3\text{OH}:\text{H}_2\text{O}$ , 50:50  $\text{CH}_3\text{OH}:\text{H}_2\text{O}$ , 100:0  $\text{CH}_3\text{OH}:\text{H}_2\text{O}$ , 50:50 dioxane: $\text{H}_2\text{O}$ , and 90:10 dioxane: $\text{H}_2\text{O}$ ) not only differ from the gas-phase equilibrium distribution but are also dramatically different from one another. Substantially greater populations of the A and B states are produced, and these solution-dependent data show many additional peaks—especially in regions beyond the  $305 \text{ \AA}^2$  limit observed for ions formed from selection and activation of states in the gas phase. In total, there are 10 reproducible peaks when all of the different solutions are considered. IMS data for some solutions (e.g., 90:10 dioxane:water) reveal that at least eight peaks are observed from a single solution. The structural differences that

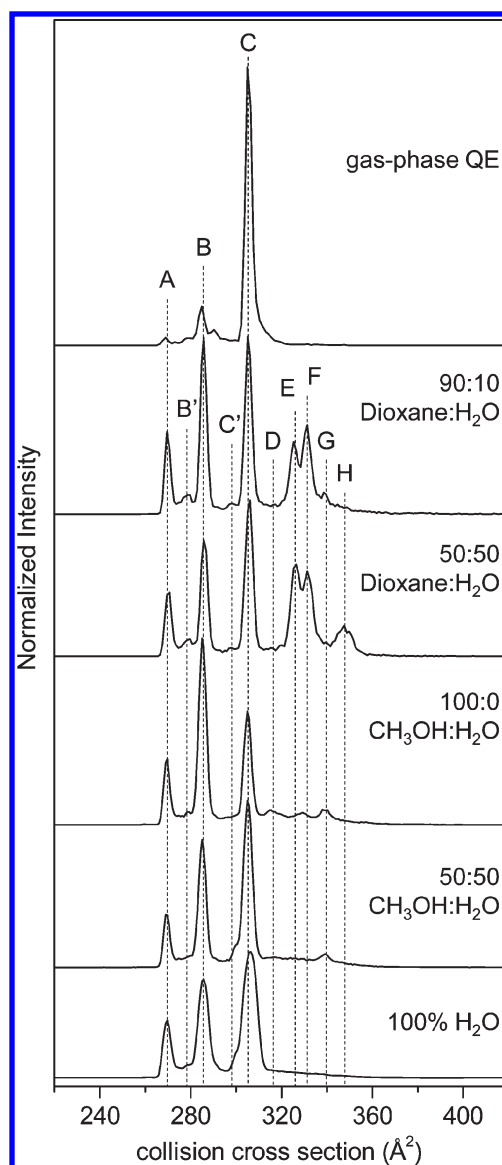


**Figure 2.** Selected  $[\text{BK}+3\text{H}]^{3+}$  collision cross section profiles for five ESI solution conditions, and the gas-phase quasi-equilibrium (QE) distribution obtained by collisional annealing of a single conformer to form peaks A–C. Dashed lines are inserted in order to guide the eye along peak centers for the 10 labeled features.

are observed for ions produced from these solutions require that transitions between states are influenced by the solvent composition.

The number of unique structures that are influenced by the solution composition can be assessed by examining the changes in peak intensities in Figures 1 and 2. This analysis is important for assessing how many unique conformations are present in solution because it rules out the possibility that multiple gas-phase ion structures originating from the same population of solution states are responsible for the large number of peaks. From studies that consider competition with  $[\text{BK}+2\text{H}]^{2+}$ , we rule out that variations in the IMS spectra for  $[\text{BK}+3\text{H}]^{3+}$  are due only to changes associated with competition between charge states. It is interesting to consider how populations may evolve toward the gas-phase equilibrium distribution in the final stages of droplet evaporation. Simulations of mixed solvent clusters

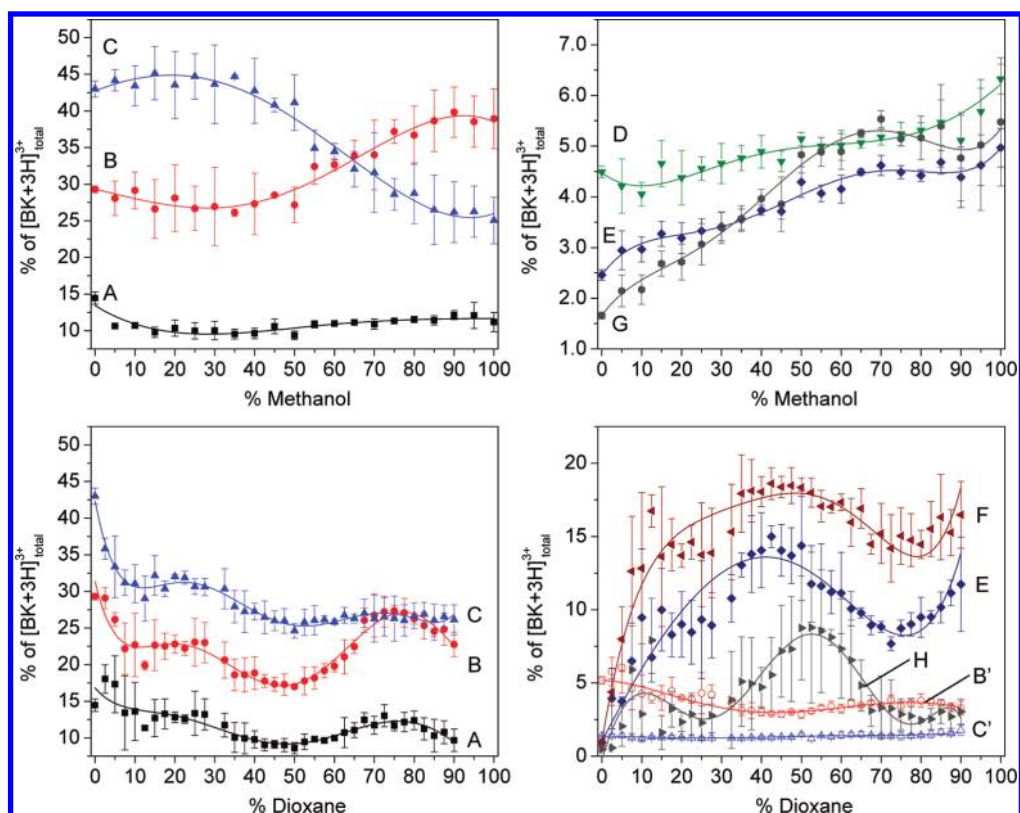


**Figure 3.** Peak integrations as a percent of the total  $[\text{BK}+3\text{H}]^{3+}$  distribution for the 10 labeled features in Figure 2. Percentage values for peaks A, B, C, D, E, and G are shown on top for the methanol:water solution set. Values for peaks A, B, C, F, E, and H and intermediate peaks B' and C' are shown below for the dioxane:water data set. Error bars represent the standard deviation from a triplicate analysis. Each set of points was fit with a polynomial function to illustrate change in conformer abundance as a function of solution composition.

show changes in solvent composition in these small droplets.<sup>21</sup> We cannot rule out such an effect here; however, our measured populations remain dependent on initial solution composition.

These arguments can be seen more clearly from the detailed analysis in Figure 3. The intensities of the largest peaks A–C vary independently with solution composition. In 100% water, the A, B, and C peaks comprise ~15, 30, and 45% of the distribution, respectively. In the methanol:water system, the relative intensity of A remains virtually unchanged as the fraction of methanol is increased, whereas peak B increases from ~25 to 40%, and peak C decreases from ~40 to 25% (as the percentage of methanol is increased from 50 to 100%). In the dioxane:water system, all three A–C peaks decrease in intensity (when dioxane is increased to ~50%), and then the A and B states increase somewhat (as dioxane is increased from 50 to 90%). These variations require that each state is present as an independent population in solution. From a similar analysis of the smaller features it appears that in every case peaks also behave independently as the solution compositions vary. In total, this analysis provides evidence for at least 10 distinct structural types across these ranges of solutions. This plurality of states is consistent with the lack of detailed structural information from conventional techniques, which are sensitive to only one, or at most a few structures. But, it also suggests that the  $\text{Arg}^1\text{--Phe}^5$  region is not completely random.

Unlike the D–H structures that are formed only from specific solutions, we find it remarkable that the A–C states can be formed in the gas phase (upon selection and ion activation) from any of the 10 resolved peaks. One explanation is that A–C emerge from solution as other structures and rapidly evolve into

these preferred gas-phase conformations. That is, there are no substantive barriers between the solution- and gas-phase conformers, and as the final solvent molecules leave the system these gas-phase structures are favored. Another interpretation is that the A–C ion structures are left unchanged during the ESI process. In this interpretation, the solvent is irrelevant in establishing structure! This conclusion is especially intriguing because each of the A, B, and C states is observed directly from every solution condition and can also be prepared in the absence of any solution. It becomes even more interesting if these large peaks not only retain but actually form the structured  $\text{Ser}^6\text{--Arg}^9$   $\beta$ -turn motif that is measurable in solution.<sup>14</sup> This idea extends several recent reports about large complexes<sup>22</sup> as well as early oligomerization steps associated with peptide aggregation,<sup>5</sup> which have suggested that these systems retain elements of solution structure in the gas phase.

Enhanced sampling molecular dynamics simulations that provide insight about candidate structures for solution-phase and dehydrated  $[\text{BK}+3\text{H}]^{3+}$  ions are valuable in guiding our explanation of these results. These simulations are analogous to calculations described elsewhere.<sup>23,24</sup> Here, we use the AMBER FF99SB all-atom force field and the GB/SA implicit solvent model to represent an aqueous environment. Dehydrated structures are generated from solution-phase candidate structures via energy minimization steps in vacuo; cross sections for dehydrated conformers that are favored are calculated using the trajectory method, available through the MOBCAL software.<sup>25</sup> This approach mimics the transition of the molecule from solution to the gas phase.<sup>26</sup> These simulations yield four populations of states, and the calculated

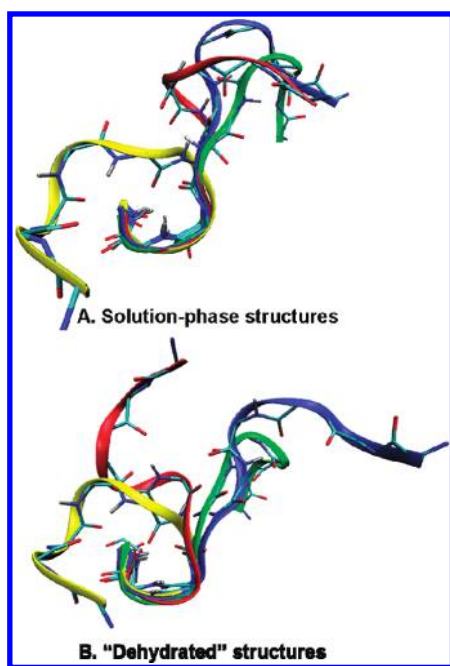


**Figure 4.** Examples of four low-energy conformations of solution-phase structures (A) and dehydrated structures (B) superimposed on the backbone atoms of Ser<sup>6</sup>–Pro<sup>7</sup>–Phe<sup>8</sup>–Arg<sup>9</sup>. Calculated cross sections of solution-phase structures are 299 (blue), 285 (red), 274 (yellow), and 296 Å<sup>2</sup> (green). Cross sections of dehydrated structures are 303 (blue), 285 (red), 271 (yellow), and 297 Å<sup>2</sup> (green).

cross sections for many low-energy structures agree with values measured for the A–C populations. Figure 4 shows representative structures from these four populations. Each candidate structure is protonated on the N-terminus and the guanidine groups of Arg<sup>1</sup> and Arg<sup>9</sup>. The solution-phase simulations appear to capture the Ser<sup>6</sup>–Arg<sup>9</sup>  $\beta$ -turn motif (in three of the four structural types), consistent with experimental measurements in solution.<sup>14,15</sup> The Arg<sup>1</sup>–Phe<sup>5</sup> region shows structural variations that arise from charge solvation of the guanidine group of Arg<sup>1</sup> by backbone carbonyl groups. Other populations (not shown) have cross sections that match the E and F peaks. These ions emerge as more elongated (almost linear) structures with each guanidine group protonated and the third proton freely migrating along the full length of the peptide. This theoretical treatment captures the idea that, upon drying, solution structures can be trapped as stable gas-phase geometries. In the case of the A–C states, the well-defined solution  $\beta$ -turn motif (Ser<sup>6</sup>–Arg<sup>9</sup>) persists, and it is the remaining region (Arg<sup>1</sup>–Phe<sup>5</sup>) that leads to distinct populations. Thus, the populations of states that are trapped upon dehydration reflect the solution composition. It is unknown to what extent the defined geometries associated with the Arg<sup>1</sup>–Phe<sup>5</sup> region that persist in the gas phase resemble the antecedent solution structures.

Regardless of whether the gas-phase structures are identical to those in solution, the current data show that it is possible to monitor populations even when regions appear “unstructured” from traditional techniques. These data underscore the importance of developing accurate, predictive computational tools that capture the transition from the solvated to the dehydrated state.

## AUTHOR INFORMATION

### Corresponding Author

clemmer@indiana.edu

## ACKNOWLEDGMENT

We gratefully acknowledge partial funding for instrumentation development from the NIH (RC1GM090797-02) and from the Indiana University METAcyte initiative that is funded by a grant from the Lilly Endowment. L.C. and D.H.R. gratefully acknowledge support for this research by the Robert A. Welch Foundation (A-1176) and the U.S. Department of Energy, Division of Chemical Sciences, BES (BES-DE-FG-04ER-15520).

## REFERENCES

- Pierson, N. A.; Valentine, S. J.; Clemmer, D. E. *J. Phys. Chem. B* **2010**, *114*, 7777.
- Fenn, J. B.; Mann, M.; Meng, C. K.; Wong, S. F.; Whitehouse, C. M. *Science* **1988**, *246*, 64.
- Hoaglund-Hyzer, C. S.; Counterman, A. E.; Clemmer, D. E. *Chem. Rev.* **1999**, *99*, 3037.
- Lee, S.-W.; Freivogel, P.; Schindler, T.; Beauchamp, J. L. *J. Am. Chem. Soc.* **1998**, *120*, 11758.
- Bernstein, S. L.; Dupuis, N. F.; Lazo, N. D.; Wytenbach, T.; Condron, M. M.; Bitan, G.; Teplow, D. B.; Shea, J. E.; Ruotolo, B. T.; Robinson, C. V.; Bowers, M. T. *Nat. Chem.* **2009**, *1*, 326.
- Abelous, J. E.; Bardier, E. *C.R. Soc. Biol.* **1909**, *66*, 511.
- Anrade, S. O.; Roche E Silva, M. *Biochem. J.* **1956**, *64*, 701.
- Boissonnas, R. A.; Guttmann, St.; Jaquenoud, P.-A. *Helv. Chim. Acta* **1960**, *43*, 1349.
- Garcia, L. J. *Handb. Exp. Pharmacol.* **1978**, *50*, 464.
- Regoli, D.; Barabé, J. *Pharmacol. Rev.* **1980**, *32*, 1.
- Hall, J. M.; Morton, I. K. M. In *The Kinin System*; Farmer, S. G., Ed.; Academic Press: San Diego, CA, 1997; pp 9–43.
- Cann, J. R.; Stewart, J. M.; Matsueda, G. R. *Biochemistry* **1973**, *12*, 3780.
- Takeuchi, H.; Harada, I. *J. Raman Spectrosc.* **1990**, *21*, 509.
- Young, J. K.; Hicks, R. P. *Biopolymers* **1994**, *34*, 611.
- Hicks, R. P. *Curr. Med. Chem.* **2001**, *8*, 627.
- Mason, E. A.; McDaniel, E. W. *Transport Properties of Ions in Gases*; Wiley: New York, 1988.
- von Helden, G.; Hsu, M. T.; Kemper, P. R.; Bowers, M. T. *J. Chem. Phys.* **1991**, *95*, 3835–3837.
- Hunter, J.; Fye, J.; Jarrold, M. F. *Science* **1993**, *260*, 784.
- Shvartsburg, A. A.; Li, F.; Tang, K.; Smith, R. D. *Anal. Chem.* **2006**, *78*, 3706.
- Koeniger, S. L.; Merenbloom, S. I.; Valentine, S. J.; Jarrold, M. F.; Udseth, H. R.; Smith, R. D.; Clemmer, D. E. *Anal. Chem.* **2006**, *78*, 4161.
- Ahadi, E.; Konermann, L. *J. Am. Chem. Soc.* **2011**, *133*, 9354.
- Ruotolo, B. T.; Giles, K.; Campuzano, I.; Sandercock, A. M.; Bateman, R. H.; Robinson, C. V. *Science* **2005**, *310*, 1658.
- Gao, Y. Q.; Yang, L. *J. Chem. Phys.* **2006**, *125*, 114103.
- Chen, L.; Shao, Q.; Gao, Y.-Q.; Russell, D. H. *J. Phys. Chem. A* **2006**, *115*, 4427.
- Mesleh, M. F.; Hunter, J. M.; Shvartsburg, A. A.; Schatz, G. C.; Jarrold, M. F. *J. Phys. Chem.* **1996**, *100*, 16082.
- Grabauer, M.; Wu, C.; Soto, P.; Shea, J. E.; Bowers, M. T. *J. Am. Chem. Soc.* **2010**, *132*, 532.